

Water Adsorption at the Tetrahedral Titania Surface Layer of $\text{SrTiO}_3(110)-(4 \times 1)$

Zhiming Wang,[†] Xianfeng Hao,[†] Stefan Gerhold,[†] Zbynek Novotny,[†] Cesare Franchini,[‡] McDermott Eamon John Gordon,[¶] Karina Schulte,[§] Michael Schmid,[†]
and Ulrike Diebold^{*,†}

*Institute of Applied Physics, Vienna University of Technology, Vienna, Austria, Faculty of Physics
& Center for Computational Material Science, University of Vienna, Vienna, Austria, Institute of
Materials Chemistry, Vienna University of Technology, Vienna, Austria, and MAX IV Laboratory,
Lund University, Lund, Sweden*

E-mail: diebold@iap.tuwien.ac.at

*To whom correspondence should be addressed

[†]Institute of Applied Physics, Vienna University of Technology, Vienna, Austria

[‡]Faculty of Physics & Center for Computational Material Science, University of Vienna, Vienna, Austria

[¶]Institute of Materials Chemistry, Vienna University of Technology, Vienna, Austria

[§]MAX IV Laboratory, Lund University, Lund, Sweden

Abstract

The interaction of water with oxide surfaces is of great interest for both fundamental science and applications. We present a combined theoretical [density functional theory (DFT)] and experimental [Scanning Tunneling Microscopy (STM), photoemission spectroscopy (PES)] study of water interaction with the two-dimensional titania overlayer that terminates the SrTiO₃ (110)-(4 × 1) surface and consists of TiO₄ tetrahedra. STM, core-level and valence band PES show that H₂O neither adsorbs nor dissociates on the stoichiometric surface at room temperature, while it dissociates at oxygen vacancies. This is in agreement with DFT calculations, which show that the energy barriers for water dissociation on the stoichiometric and reduced surfaces are 1.7 and 0.9 eV, respectively. We propose that water weakly adsorbs on two-dimensional, tetrahedrally coordinated overlayers.

1. Introduction

The discovery of photochemical water splitting on SrTiO₃ with no external bias under UV irradiation has motivated much research into the interaction of water with this material.^{1,2} More recent reports of overall water splitting on SrTiO₃ with a NiO co-catalyst has renewed this interest.^{3,4} A fundamental question is simply whether water adsorption is molecular or dissociative.^{5–13} For SrTiO₃(001), photoemission spectroscopy (PES), high-resolution electron energy loss spectroscopy (HREELS) and temperature programmed desorption (TPD) studies show that water does not adsorb on the stoichiometric surface at room temperature (RT) although molecular water adsorption has been observed below 150 K. However, dissociative adsorption was observed for water on both, Ar⁺ bombarded and vacuum-fractured SrTiO₃(100) surfaces.^{10–12} Theoretical calculations are in agreement with experimental results, predicting molecular water adsorption on the stoichiometric SrTiO₃(100) surface.^{14–16}

In this context it is important to note that SrTiO₃(100) forms a wide variety of reconstructions, which depend strongly on the preparation conditions and sample history. Various groups report different results,¹⁷ thus it is not always straightforward to connect water adsorption experiments

to the actual surface structure. Recently the SrTiO₃(110) surface has received significant attention.^{18–22} It was found that SrTiO₃(110) surface can be prepared reproducibly and reversibly with a variety of surface structures.^{18,20} The ($n \times 1$) ($n = 3 - 6$) series of reconstructions was solved by transmission electron diffraction and direct methods, and confirmed and refined by density functional theory (DFT) calculations and scanning tunneling microscopy (STM).^{19,21} Thus a reliable structural model is available for this surface.

The SrTiO₃(110) surface is polar, as an SrTiO₃ crystal can be considered as a stack of equidistant (SrTiO)⁴⁺ and (O₂)⁴⁻ planes along the [110] direction.²³ Generally, polar surfaces are considered more reactive than non-polar ones.^{24,25} In this case, however, the polarity is compensated via the formation of a (4×1) reconstruction with a nominal stoichiometry of (Ti_{1.5}O₄)²⁻. The reconstruction consists of six- and ten-membered rings of corner-shared TiO₄ tetrahedra residing directly on the bulk-like SrTiO₃, which consists of octahedrally-coordinated Ti (see Fig. 1a). The surface reconstruction can be tuned by varying the surface stoichiometry,^{20,26} forming a homologous series of ($n \times 1$) ($n = 3 - 6$) with a variable number of tetrahedra per ring.^{19,21} Recently, we reported that quasi-long-range ordered antiphase domains are formed on the (4×1) surface.²⁷ The domain boundaries are decorated by defect pairs consisting of a Ti₂O₃ vacancy cluster and a Sr adatom; the presence of these pairs preserves the polarity compensation.

In recent reports, periodically-arranged, tetrahedrally coordinated MeO₄ (Me = Ti, Si) units have emerged as a common feature on several oxide surfaces.^{19,21,28–31} For example, such units form one-dimensional rows at the anatase TiO₂(001)-(1 × 4) and rutile TiO₂(110)-(1 × 2)-Ti₂O₃ surfaces.^{28,29} For anatase (001) a high reactivity towards water adsorption was reported;^{32,33} this surface was also identified as the most active one in photocatalytic reactions,³⁴ although it remains controversial whether the reconstructed or the unreconstructed anatase (001) surface is the most active phase.³⁵ Well-ordered, ultrathin silica structures consisting of SiO₄ units have also been reported³⁶ these bear resemblance to the two-dimensional network on the SrTiO₃(110)-($n \times 1$)($n = 3 - 6$) and rutile TiO₂(100)-*c*(2 × 2) surfaces.^{19,21,31} It should be noted, however, that Ti in bulk TiO₂ and SrTiO₃ is octahedrally coordinated, in contrast to SiO₂, which forms tetrahedra also in

the bulk.

In this article we present a combined experimental [Scanning Tunneling Microscopy (STM), photoemission spectroscopy (PES)] and theoretical [density functional theory (DFT)] investigation of water adsorption on stoichiometric and reduced SrTiO₃(110) surfaces with a two-dimensional tetrahedrally-coordinated (4×1) reconstructed layer. Both experimental and theoretical results clearly show that water dissociates on the surface with oxygen vacancies (V_O 's), while water neither adsorbs nor dissociates on the stoichiometric surface at room temperature (RT). Generalizing our result we propose that two-dimensional, tetrahedrally coordinated overlayers on oxide materials interact only weakly with water.

2. Materials and Methods

2.1 Experimental Details

STM measurements were performed in two ultra-high vacuum (UHV) chambers equipped with a SPECS Aarhus STM at RT and an Omicron low temperature (LT) STM at 78 K, respectively (see Refs 37 and 38 for more details). Synchrotron radiation photoemission spectroscopy experiments were performed at beamline I311 at the MAX IV Laboratory.³⁹ The pressure in all UHV systems was better than 1×10^{-10} mbar. Nb-doped (0.5 wt%) SrTiO₃(110) single crystals were purchased from MaTeck, Germany. The clean surface was prepared by cycles of Ar⁺ sputtering (1 keV, 5 μ A, 10 minutes) and followed by annealing in 2×10^{-6} mbar oxygen at 900 °C for 1 h.⁴⁰ The samples were heated by electron bombardment (13 mA, 900 V) or by passing alternating current through the crystal, and the temperature was monitored with an infrared pyrometer. The surface reconstruction was checked by low energy electron diffraction (LEED) and was adjusted by depositing Sr or Ti on the surface at RT followed by annealing until a sharp (4×1) LEED pattern was observed.²⁰ The surface was exposed to atomic H by backfilling the chamber with H₂ while keeping a hot tungsten filament in line of sight with the sample. The hydrogen cracking efficiency in our setup is estimated 5% with the W filament temperature about 2000 °C.⁴¹ The density of H atoms is around

0.1 per nm² after dosing at a H₂ partial pressure of 1×10^{-6} mbar for 5 min with the sample at room temperature. Deionized H₂O was cleaned by repeated freeze-pump-thaw cycles and dosed by backfilling the UHV chamber through a leak valve. The purity of the water vapor was checked by mass spectrometry. All photoemission spectra in this paper were collected with the emission normal to the sample plane; the angle between the sample normal and the incoming x-rays was 54.7°. Photon energies were 605 eV and 45 eV for core-level and valence band photoemission spectroscopy, respectively. The binding energies were calibrated with respect to the Fermi level of a clean Mo sample plate, on which our sample was mounted.

2.2 Computational Details

The first-principles calculations were performed using the projector augmented-wave method as implemented in the Vienna *ab initio* simulation package (VASP) code,^{42,43} using the Perdew-Burke-Ernzerhof (PBE)⁴⁴ approximation to treat the exchange-correlation functional within the DFT. The kinetic energy cutoff for the plane waves expansion was set to 600 eV, and reduced to 400 eV for the nudged elastic band (NEB) calculations as detailed below. In order to improve the description of dispersion forces, which are expected to play an important role in H₂O physisorption phenomena and are not correctly accounted for in standard DFT, we have employed two alternative corrections: (i) the DFT-D2 method of Grimme^{45–47} and (ii) the modified version of van der Waals DFT (vdW-DFT), adopting the recently introduced functional optB86b-vdW.⁴⁸

Our surface calculations are based on the SrTiO₃(110)-(4 × 1) structural model proposed by Enterkin *et al.*¹⁹ To weaken the interaction between the water and its periodic image we have adopted a large (4 × 2) supercell (Fig. 1), which is constructed by doubling the (4 × 1) model along the [1 $\bar{1}$ 0] direction. We have used a symmetric slab consisting of 13 layers separated by a vacuum layer of 12 Å (total thickness 32 Å). A pair of H₂O molecules was symmetrically adsorbed on both sides of the slab. During structural optimization all atoms were allowed to relax until all components of their residual forces were less than 0.02 eV/Å, except for the atoms in the central three layers, which were kept fixed in their bulk positions. We have used the fully optimized

PBE lattice constant, 3.945 Å (very close to the corresponding experimental one, 3.905 Å), and a $(2 \times 3 \times 1)$ Monkhorst-Pack k-point mesh (reduced to $1 \times 1 \times 1$ for the NEB runs) for the Brillouin-zone integrations.

The oxygen vacancy formation energy $E_f(V_O)$ is computed as $E_f(V_O)=1/2[E_{TOT}(2V_O)-E_{TOT}+E(O_2)]$ where E_{TOT} refers to the DFT total energy of the clean symmetric slab, $E_{TOT}(2V_O)$ denotes the DFT total energy of the symmetric slab containing two V_O 's, and $E(O_2)$ indicates the DFT energy of the oxygen molecule. Similarly, the H and H_2O adsorption energies are evaluated using the formula $E_{ads}(X)=1/2[E_{TOT}(2X)-E_{TOT}-2E(X)]$ (with $X=H$ and H_2O), where $E_{TOT}(X)$ refers to the DFT total energies of the symmetric slab containing two H atoms or two water molecules, whereas $E(X)$ represents the DFT energies of the isolated H atom or H_2O molecule.

The energy barriers for the water dissociation processes were determined via the climbing image NEB (CI-NEB) method,⁴⁹ which is designed to compel one of the intermediate states near the transition point to climb up along the reaction coordinate to reach the highest saddle point, thus leading to a more accurate evaluation of the energy barrier than the regular NEB does. Due to the computational load, we adopted 4-8 images connecting two subsequent minima of the potential energy surface for determining the minimum energy path. The whole path was considered to be converged when the residual forces acting on the individual images dropped below the threshold of 0.05 eV/Å. For the NEB calculations we did not include dispersion corrections on top of DFT, as it has been demonstrated that these have little impact on the activation energy.⁵⁰

3. Results

3.1 Scanning Tunneling Microscopy Studies

Figure 2a shows an empty-states STM image of the $SrTiO_3(110)$ surface after exposure to atomic hydrogen at an H_2 pressure of 1×10^{-6} mbar for 5 min. The bright stripes along the $[1\bar{1}0]$ direction correspond to the Ti(III) and Ti(II) atoms in the six-membered rings, located in tetrahedral units that connect to the $SrTiO_3$ substrate below by sharing corners. The ridges are separated by a

dark trench originating from the tetrahedra in the ten-membered rings, which share edges with the SrTiO₃ underneath (see Fig. 1). Each stripe contains two or three bright rows of periodic dots for the (4 × 1) or (5 × 1) reconstruction, respectively.²¹ On top of the stripes, two types of bright protrusions are observed. Sr adatoms, which are part of the (4 × 1) antiphase domain structure²⁷ are labeled with red arrows. In agreement with the DFT calculations²⁷ they are adsorbed in the middle of the six-membered rings, *i.e.*, centered on the bright (4 × 1) stripes. The Sr adatoms have an apparent height of ~240 pm. [Quoted here and in the following are typical values for the apparent heights observed for an STM sample bias of +2.3 V and a tunneling current of 0.1 nA. Note however, the apparent height also depends on the tip state.]

It is well accepted that atomic hydrogen preferentially adsorbs on the surface oxygen atoms, forming hydroxyl groups.⁵¹⁻⁵⁴ In our case, the hydroxyl groups (labeled with white arrows in Fig. 2a) have an apparent height of ~130 pm, less than the Sr adatoms. The OH groups appear preferentially at the sides of both, the (4 × 1) and (5 × 1) stripes. DFT calculations (below) show that atomic hydrogen prefers to adsorb at the O3 site (Fig. 1), and the resulting simulated STM image is consistent with experimental results.²¹ It should be noted that we also observed indications of H interaction with Sr adatoms; note, *e.g.*, the streaky appearance of the extra-bright Sr atom in Fig. 2a that indicates the presence of an adsorbate.

After flashing the hydroxylated surface to about 300 °C, less bright protrusions with an apparent height of ~70 pm appear (blue arrows in Fig. 2b). From TPD and STM experiments it is often observed that molecular water desorbs from hydroxylated oxide surfaces upon flash-annealing.^{37,51,52} Indeed, from a prior TPD study a similar conclusion was drawn for the SrTiO₃(001) surface.¹³ It was observed that molecular water desorbs above 100 °C on the hydroxylated SrTiO₃(001) surface.¹³ Therefore, it is reasonable to attribute the less bright protrusions to V_O's. The V_O's sit also at the side of the (4 × 1) stripes, similar to the hydroxyls. These results agree very well with the preference for a V_O at the O3 site in DFT calculations as shown in the following and in Ref. 21.

Figure 3a shows an LT-STM image of the SrTiO₃(110) surface after exposure to 0.3 Langmuir

(L) water at 110 K. Bright features with an apparent height of ~ 80 pm, labeled with green arrows, appear in the trenches between stripes. These features are different from the V_O 's and hydroxyls in Fig. 2. From TPD measurements on the $\text{SrTiO}_3(001)$ surface, molecular water starts to desorb around 200 - 260 K at low exposure (< 1 L), while weakly bound and multilayer water desorbs below 200 K upon further exposure.¹³ We attribute the features in Fig. 3a to molecular water that is located at the cation sites at low exposure. From the DFT calculations shown below, molecular water preferentially adsorbs at the TiI site in the ten-membered rings on the $\text{SrTiO}_3(110)-(4 \times 1)$ surface (Fig. 1b), consistent with the experimental observations. (5×1) stripes (Fig. 3b), indicating hydroxyl formation after dosing water at RT. In addition to single hydroxyls, hydroxyl pairs are also observed on the surface, again labeled by white arrows in Fig. 3b. These pairs are likely due to the dissociation of water at the V_O 's. Note that the distance between these hydroxyl pairs is two unit cells along direction, indicating a repulsive interaction between them. Here the saturation coverage of hydroxyls is approximately 0.01 ML (1 ML = 4.64×10^{14} atoms/cm² relative to the $\text{SrTiO}_3(110)-(1 \times 1)$ unit cell), suggesting a surface V_O density of half that value. Further increasing the water dosage up to 50 L does not introduce more hydroxyls on the surface, and no indication of molecular water is observed. We conclude that water dissociates only on the V_O 's while it neither adsorbs nor dissociates on the stoichiometric surface at RT.

3.2 Photoemission Spectroscopy Studies

Figure 4 shows photoemission spectra of the valence band region of differently treated $\text{SrTiO}_3(110)$ surfaces. The valence band of the clean surface shows mainly O $2p$ -derived features. By linearly extrapolating the onset of the spectra, the valence band maximum (VBM) is determined to be located at 3.2 eV below the Fermi level (E_F), in agreement with the Nb-doped n -type sample and a reported band gap of 3.2 eV for SrTiO_3 .⁵⁵ For the clean surface no states are observed in the band gap region,⁵⁶ indicating that Nb dopants do not induce in-gap states. This is consistent with the picture that the band structure of lightly n -type doped samples can be well described by a simple rigid band shift.⁵⁷

After dosing up to 240 L water on the clean surface at RT, the valence band spectrum does not change compared to that of the clean surface. For molecularly adsorbed water one would expect features related to its $1b_2$, $3a_1$ and $1b_1$ orbitals.⁵⁸ On the other hand, an OH 3σ state as well as in-gap states can be observed when dissociative adsorption occurs.^{6–10,59} In experiments on as-dosed samples, we did not observe any features related to molecular and dissociative water, in agreement with the conclusion of a rather unreactive surface drawn on the basis of our STM results.

After dosing atomic hydrogen, an in-gap state with a binding energy of 1.3 eV is observed, as well as a feature state below the O $2p$ valence band. Partially this feature can be assigned to the OH 3σ state, which is located at 10.8 eV.⁶⁰ At first sight, the higher binding energy features could be associated with water $1b_2$ and $3a_1$ states. However, water does not adsorb on the clean surface at RT, as shown in our STM measurements. Furthermore, no features were observed related to molecular water from the O $1s$ core-level spectrum for the H-exposed surface (Fig. 5). Instead, STM indicates that H interacts with the Sr adatoms. We tentatively attribute the higher binding energy features to states related to Sr-OH species.^{11,12} An in-gap state appears after creating V_O 's on the clean surface by exposing the surface to intense synchrotron radiation. After exposure to synchrotron light a similar in-gap state and related two-dimensional electron gas were observed on SrTiO₃(001) and other perovskite surfaces,^{57,61,62} as well as TiO₂ surfaces.⁵⁰ We find that the in-gap state can be quenched after exposure to O₂ at RT, supporting that it arises from V_O 's.⁵⁷

When exposing the surface with V_O 's to 1.2 L water at RT, the in-gap state hardly changes. However, a well-defined OH 3σ state with a binding energy of 10.8 eV is observed, which indicates water dissociation and formation of hydroxyls. It is well-known that the presence of hydroxyls results in a similar in-gap state as O vacancies.⁵⁸ This supports the conclusion that water dissociates on the reduced surface.

Similar conclusions are drawn from the corresponding O $1s$ core-level photoemission spectra (Fig. 5). The O $1s$ spectrum obtained on the clean surface shows a slightly asymmetric peak shape with the main peak located at 530.2 eV and a small shoulder at a higher binding energy of 531.7 eV. The spectrum does not change after dosing water on the clean surface at RT. After dosing atomic

hydrogen and water on the reduced surface, the ratio increases slightly. This result is consistent with observations on titania surface.^{63–65}

3.3 Electronic Structure Calculations

To complement the photoemission spectra and achieve an understanding of the electronic properties of the defective and hydroxylated surface as compared to the clean (4×1) one, we have determined the most stable configurations and computed their density of states (DOS). By comparing the energies of all possible inequivalent configurations, we determined the most favorable site for the formation of a V_O and for hydrogen adsorption.

The results, collected in Table 1, show that O3 has the lowest V_O formation energy, in agreement with a recent first-principles study²¹ and consistent with our STM measurements (Fig. 2b). It also represents the most favorable hydrogen adsorption site, with an adsorption energy of 2.19 eV. The most stable hydroxyl is characterized by an O-H bond length of 0.983 Å, slightly larger than that of a free OH group (0.97 Å), and a 45.1° angle with respect to the surface normal.

We have calculated the DOS of the most favorable oxygen-defective and hydroxylated surfaces. The results are compared to the clean (4×1) surface in Fig. 6. Given the well-known drawbacks of standard (local and semilocal) DFT functionals in predicting the correct electronic ground state of strongly correlated electron systems and in describing electron localization effects, we have computed the DOS by means of the PBE+U method,⁶⁶ using an effective on-site Coulomb repulsion $U_{\text{eff}} = 4.6$ eV for the Ti d states, a choice in line with previous studies.⁶⁷ The most relevant feature of the V_O case is the appearance of a midgap state right above the valence band maximum, in agreement with the photoemission data. This state originates from the Ti^{3+} atoms adjacent to the V_O , which locally trap the extra electrons created by the V_O . The adsorption of one OH group leads to the formation of only one Ti^{3+} , and to the emergence of a feature at about -7 eV below the VBM. This feature is attributed to the OH- 3σ bonding state, as shown in the inset of Fig. 6. This picture is reminiscent of the one found for the rutile $\text{TiO}_2(110)$ surface.^{68–70}

3.4 DFT Calculations: Interaction with H₂O

To elucidate the adsorption of water on the SrTiO₃(110)-(4 × 1) surface and to examine the role of V_O's we have performed NEB calculations. One important question is whether the water is predicted to adsorb molecularly or dissociatively on the SrTiO₃(110) surface. To answer this question we have investigated the energetics of different adsorption configurations at low coverage, both in molecular and dissociated form, as well as the dissociation energy barriers/pathways among the different configurations. We first focus on the interaction between water and the clean (4 × 1) surface and then we discuss the results obtained for the reduced surface.

3.4.1 Ideal Surface + H₂O

Molecular adsorption. Our first concern is to identify locally stable molecular H₂O configurations. We have scrutinized several possible adsorption sites at a coverage of 1/8 ML [one H₂O molecule per (4 × 2) unit cell].

The most favorable adsorption site is located in the ten-membered rings near TiI, as shown in the insets of Fig. 7. The distance between TiI and the water oxygen atom (O_W) is found to be 2.341, 2.325 and 2.311 Å with the PBE, DFT-D2 and vdW-DFT functional, respectively. The corresponding water adsorption energies E_{ads}(H₂O) are -0.716, -1.014 and -1.073 eV, respectively. As expected, the van der Waals correction substantially increases the magnitude of the adsorption energy, although the geometries are similar to the standard PBE case. Moreover, the other configurations considered are less stable by 0.15 - 0.5 eV. Both the H-O_W bond length (1.00 Å) and the H-O_W-H bond angle (106°) are almost identical to the corresponding values in the free water molecule, 0.985 Å and 104.96°, respectively. We also evaluated adsorption energies at the experimental condition (300K and 10⁻⁹ atm) within the framework of *ab initio* thermodynamics.^{71,72} The corresponding values are +0.482, 0.184 and 0.125 eV with the PBE, DFT-D2 and vdW-DFT, respectively. The positive value indicates that water does not adsorb on the ideal surface, in agreement with experiment.

Dissociative adsorption. To explore the dissociative configuration (coadsorption of H and OH

species), which serves as a basis for studying the water dissociation process, we assumed that the OH species preferentially adsorbs on the Ti atom, and the H atom on the neighboring/next-neighboring surface O atoms. This assumption is reasonable, as no local minimum corresponding to an adsorption at the surface Ti site was found for the H atom.

Most of the dissociative adsorption configurations we explored are unstable (*i.e.* with positive adsorption energy), or relax to the molecular pattern. We established only five stable/metastable dissociative patterns with negative/zero adsorption energy. As mentioned before, here we performed the calculations with the PBE functional, since application of DFT-D2 and vdW-DFT does not alter the adsorption sequence and the geometries. The computed adsorption energy for the most stable pattern is -0.779 eV, about 60 meV more stable than the molecular adsorption case. In the latter configuration (not shown), the OH species anchors on the bridge site between the two Ti surface atoms (TiII and TiIII), while the atom O3, bonded to another H atom, shifts downward due to the electrostatic potential repulsion; this results in two five-fold coordinated Ti atoms.

On the basis of the computed adsorption energies alone we cannot unambiguously determine whether water molecules are predicted to adsorb molecularly or dissociatively on the SrTiO₃(110)-(4 × 1) surface. We have conducted a series of CI-NEB calculations in order to model the dynamics.

Dissociative reaction. We have determined the energy barrier for the water dissociation processes from the most stable molecular adsorption state (initial state) to the geminate dissociative state (final state) by using the CI-NEB method. This procedure allows us to find the minimum energy reaction paths. This pathway choice is appropriate when the strongest molecular adsorption is considered, as in the present case. The resulting energy profile together with the representative structural models is shown in Fig. 7. The transition barrier for the H₂O to dissociate on the SrTiO₃(110)-(4 × 1) surface is rather large (> 1.6 eV), much higher than the adsorption energies of both the molecularly or dissociated state. This clearly shows that the H₂O molecule is not predicted to dissociate on the defect-free surface, in agreement with the experimental observations.

3.4.2 Reduced Surface + H₂O

As mentioned in the experimental section, significant amounts of hydroxyls are found on the SrTiO₃(110)-(4 × 1) surface with V_O's after dosing water. This suggests that the oxygen deficient surface is active with respect to water dissociation.

The water adsorption energies computed within PBE, DFT-D2 and vdW-DFT are listed in Table 2. All three methods yield very similar values of 1.7 eV, substantially larger (by about 1 eV) than those on the stoichiometric, non-defective surface. The adsorption of water on the defective surface is clearly favorable. Van der Waals interactions do not play a significant role, which is suggestive of a primarily chemisorption process.

Considering that the three different methods also deliver a quantitatively similar description of the structural characteristics (see Table 2), we will focus on the PBE results only in the following. The structural model of the optimized initial configuration is provided in Fig. 8. In the optimized structure, the H₂O molecule is slightly tilted towards one of the threefold-coordinated Ti atoms near the V_O, forming two asymmetric Ti-O_W bonds of 2.107 and 3.090 Å. One of the H-O_W bonds in the adsorbed water molecule points towards the O4 atom forming an H-bond with a bond length of 1.571 Å, in turn slightly enlarging the molecular H-O_W bond length to 1.055 Å. The second H remains free, connected to the O_W with the corresponding H-O_W bond length (0.985 Å).

As aforementioned, we primarily focus on the original geminate dissociative states. The OH species occupies the O3 vacancy site, with the remaining H atom anchored to the neighboring O4 atom (see inset in Fig. 8). The resulting O4-H is nearly flat-lying and is H-bonded with the adjacent O4' surface oxygen atom. This structural and chemical environment results in a large adsorption energy of 2.28 eV. This is already a strong indication that the water molecule is preferentially adsorbed dissociatively rather than molecularly. However, exothermicity is a necessary, but not sufficient, condition for dissociation. In order to gain more insights into the dissociative adsorption process we have conducted NEB calculations for the energy barrier. The resulting energy profile for the dissociation pathway in Fig. 8 shows an energy barrier at the transition state of 0.9 eV. This barrier is significantly lower than the corresponding values (1.7 eV) obtained on the ideal

surface, clearly indicating that V_O 's strongly facilitate water dissociation. This is again in excellent agreement with the experimental observations, which reveal that water interacts with V_O 's, forming two hydroxyl groups on the surface. Similar energy pathways for the dissociative process were also found for the defective surface with an O4 vacancy, which is characterized by an exothermic energy of 1.4 eV and a slightly larger barrier of 1.1 eV. Given the theoretical and experimental results above, it is clear that V_O 's facilitate water dissociation on the $\text{SrTiO}_3(110)$ surface and the barriers are low enough for this process to happen at room temperature or slightly above RT.

4. Discussion

Our DFT calculations show that the V_O 's are preferentially created at the O3 site in the six-membered ring of the (4×1) reconstruction, which is also the most favorable site to form OH. This is in excellent agreement with the experimental STM images (Fig. 2). Moreover, the water tends to adsorb molecularly at the TiI site in the ten-membered ring, where it appears as bright protrusions between the stripes in the STM images at low temperature (Fig. 3a).

The situation is different when water is dosed in the presence of V_O 's. Both the experimental and theoretical results unequivocally show that water dissociates spontaneously at the V_O 's at finite temperatures. In STM the two OH groups resulting from a dissociated water molecule were observed far away from each other. The DFT calculated energy barrier for the direct H diffusion is ~ 1.35 eV, indicating that the direct hopping is not possible at RT. Possibly these OH groups are driven apart via the water-assisted mechanism reported in Refs [73, 74].

Overall, the ideal, non-defective $\text{SrTiO}_3(110)-(4 \times 1)$ surface is remarkably inert towards water adsorption, while the V_O 's facilitate bonding and dissociation of water. Moreover, V_O 's created on the $\text{SrTiO}_3(110)$ surface are metastable, inclined to diffuse to subsurface sites as suggested in previous studies.²¹ Therefore, under real-world conditions we expect vacancy-mediated adsorption and dissociation to be rare on this surface.

As stated in the introduction section, $\text{SrTiO}_3(110)$ is a polar surface, consisting of alternating

(SrTiO)⁴⁺ and (O_2)⁴⁻ planes in the bulk. While an uncompensated polar surface is unstable and chemically active, our results indicate that, in this case, compensating polarity with the reconstruction network is very efficient in creating an inert surface. The most peculiar structural feature of the reconstruction is the presence of the TiO_4 tetrahedra on the top layer. Interestingly, the TiI-tetrahedra (edge-sharing with the substrate) in the ten-membered rings are reminiscent of a similar configuration at the reconstructed anatase $\text{TiO}_2(001)-(1 \times 4)$ surface,²⁸ which contains a distorted TiO_4 tetrahedron. It was demonstrated that water dissociates spontaneously on the ridge of this reconstructed surface in theoretical and experimental studies.^{32,33} In fact, the anatase $\text{TiO}_2(001)$ surface is considered the most active facet in photocatalytic reactions.³⁴ An analysis of our results gives insights as to why the TiO_4 tetrahedra are so inert in the case of $\text{SrTiO}_3(110)-(4 \times 1)$.

Electronic Aspects. While excess electrons located at the energies near the band gap of reducible oxide surfaces are generally connected with a high reactivity,⁷⁵ the clean $\text{SrTiO}_3(110)-(4 \times 1)$ surface has no in-gap states in both, experiment and theory. In fact, an analysis of the layer-resolved DOS (not shown) indicates that the top layer has a slightly larger band gap, compared to the SrTiO_3 layers underneath. In spite of the 4-fold coordination in this tetrahedral configuration, the Ti atom should not be considered undersaturated. The Ti atom hybridizes with the four surrounding oxygen atoms, forming strong covalent bonds with a short bond length, which lead to the relatively large band gap. Experimental and theoretical results also show that the Ti valence is 4+ and no in-gap state is present on the anatase $\text{TiO}_2(001)-(1 \times 4)$ surface.^{28,76} Thus, while explaining our inert $\text{SrTiO}_3(110)-(4 \times 1)$ surface, the electronic structure provides no argument for the supposedly reactive TiO_4 tetrahedra on anatase.

Interestingly, similar tetrahedrally coordinated TiO_4 units are present on the $\text{TiO}_2(110)-(1 \times 2)$ surface, forming one-dimensional Ti_2O_3 rows.²⁹ Due to the presence of Ti^{3+} species the $\text{TiO}_2(110)-(1 \times 2)$ surface is proposed to be chemically active, as demonstrated by reacting with NO .⁷⁷ It would be interesting to test whether this surface is also reactive for water dissociation.

Structural Aspects. What is needed for strong water interaction are freely accessible acidic sites, and a neighboring O atom that can act as Brønsted base (proton acceptor). In our case, the

TiO₄ tetrahedron is quite regular: the bond length ranges from 1.826 to 1.896 Å, with a O-Ti-O bond angle range of 92.82 -123.08°. The acidic Ti sites are significantly recessed into the surface compared to the surrounding oxygen atoms, making them inaccessible and non-reactive. In contrast, on the anatase TiO₂(001)(1 × 4) reconstructed surface, the TiO₄ tetrahedron is very distorted; the bond length along the [100] direction consists of alternating long (2.134 Å) and short (1.831 Å) Ti-O bonds, while the bonds along the [010] directions are identical (1.805 Å). The O-Ti-O bond angle along the [100] and the [010] direction is 145.15° and 104.76°, respectively,³² leading to the exposure of the Ti atom as an active acidic site. Furthermore, and at variance with what was found for SrTiO₃(110)-(4 × 1), the distorted TiO₄ tetrahedron on the anatase TiO₂(001)(1 × 4) surface forms a quasi-one dimensional row along the [100] direction. This flexible framework provides the freedom of relaxation, and facilitates the water dissociation. At the SrTiO₃(110)-(4 × 1) surface, the two-dimensional nesting of the six- and ten-membered rings is more rigid, which contributes to its inertness.

A similar two-dimensional reconstructed overlayer consisting of corner-sharing TiO₄ regular tetrahedra has been established on the rutile TiO₂(100)-*c*(2 × 2) surface.³¹ From the present results, we would expect this reconstructed surface also to be relatively inert; it would be interesting to test this prediction.

5. Summary and Conclusion

We have performed a systematic study of water interaction with the two-dimensional titania overlayer consisting of TiO₄ tetrahedra, on the SrTiO₃(110)-(4 × 1) surface with and without oxygen vacancies. We found that water dissociates on the oxygen vacancies, in line with many other oxide surfaces. We also found the two-dimensional, tetrahedrally coordinated TiO₄ overlayer to be remarkably inert, in contrast to the one-dimensional, tetrahedrally coordinated TiO₄ units at the anatase TiO₂(001)-(1 × 4) surface. The weak water adsorption on this surface stems from the regular tetrahedra and the two-dimensional rigid network, as well as its insulating electronic structure.

Recently, TiO_4 tetrahedra have emerged as a common building block on many Ti-containing oxides surfaces. We expect that our conclusions of a inert two-dimensional top layer should also apply to these newly-discovered surfaces.

Acknowledgement

This work has been supported by the Austrian Science Fund (FWF) under Project No. F45 and the ERC Advanced Research Grant ‘OxideSurfaces’. E.M. acknowledges support from the FWF under Project No. W1243 (Solids4Fun). All DFT calculations were performed at the Vienna Scientific Cluster (VSC-2). Valuable discussions with Annabella Selloni and Laurence Marks are gratefully acknowledged.

References

- (1) Mavroides, J. G.; Kafalas, J. A.; Kolesar, D. F. Photoelectrolysis of Water in Cells with SrTiO_3 Anodes. *Appl. Phys. Lett.* **1976**, *28*, 241–243.
- (2) Wrighton, M. S.; Ellis, A. B.; Wolczanski, P. T.; Morse, D. L.; Abrahamson, H. B.; Ginnley, D. S. Strontium Titanate Photoelectrodes. Efficient Photoassisted Electrolysis of Water at Zero Applied Potential. *J. Am. Chem. Soc.* **1976**, *98*, 2774–2779.
- (3) Townsend, T. K.; Browning, N. D.; Osterloh, F. E. Nanoscale Strontium Titanate Photocatalysts for Overall Water Splitting. *ACS Nano* **2012**, *6*, 7420–7426.
- (4) Townsend, T. K.; Browning, N. D.; Osterloh, F. E. Overall Photocatalytic Water Splitting with NiO_x - SrTiO_3 - A Revised Mechanism. *Energy Environ. Sci.* **2012**, *5*, 9543–9550.
- (5) Henrich, V. E.; Dresselhaus, G.; Zeiger, H. Chemisorbed Phases of H_2O on TiO_2 and SrTiO_3 . *Solid State Comm.* **1977**, *24*, 623 – 626.
- (6) Ferrer, S.; Somorjai, G. UPS and XPS Studies of the Chemisorption of O_2 , H_2 AND H_2O

- on Reduced and Stoichiometric SrTiO₃(111) surfaces; The Effects of Illumination. *Surf. Sci.* **1980**, *94*, 41 – 56.
- (7) Webb, C.; Lichtensteiger, M. UPS/XPS Study of Reactive and Non-Reactive SrTiO₃(100) Surfaces: Adsorption of H₂O. *Surf. Sci.* **1981**, *107*, L345 – L349.
- (8) Egdell, R.; Naylor, P. The Adsorption of Water on SrTiO₃(100): A Study of Electron Energy Loss and Photoelectron Spectroscopies. *Chem. Phys. Lett.* **1982**, *91*, 200 – 205.
- (9) Cox, P.; Egdell, R.; Naylor, P. HREELS Studies of Adsorbates on Polar Solids : Water on SrTiO₃(100). *J. Electron Spectrosc. Relat. Phenom.* **1983**, *29*, 247 – 252.
- (10) Eriksen, S.; Naylor, P.; Egdell, R. The Adsorption of Water on SrTiO₃ and TiO₂: A Reappraisal. *Spectrochim. Acta Mol. Spectrosc.* **1987**, *43*, 1535 – 1538.
- (11) Brookes, N.; Thornton, G.; Quinn, F. SrTiO₃(100) Step Sites as Catalytic Centers for H₂O Dissociation. *Solid State Comm.* **1987**, *64*, 383 – 386.
- (12) Brookes, N. B.; Quinn, F. M.; Thornton, G. The Involvement of Step and Terrace Sites in H₂O Adsorption on SrTiO₃(100). *Phys. Scr.* **1987**, *36*, 711 – 714.
- (13) Wang, L.-Q.; Ferris, K.; Herman, G. Interactions of H₂O with SrTiO₃(100) Surfaces. *J. Vac. Sci. Technol. A* **2002**, *20*, 239–244.
- (14) Azad, S.; Engelhard, M. H.; Wang, L.-Q. Adsorption and Reaction of CO and CO₂ on Oxidized and Reduced SrTiO₃(100) Surfaces. *J. Phys. Chem. B* **2005**, *109*, 10327–10331.
- (15) Baniecki, J. D.; Ishii, M.; Kurihara, K.; Yamanaka, K.; Yano, T.; Shinozaki, K.; Imada, T.; Kobayashi, Y. Chemisorption of Water and Carbon Dioxide on Nanostructured BaTiO₃-SrTiO₃(001) Surfaces. *J. Appl. Phys.* **2009**, *106*, 054109.
- (16) Guhl, H.; Miller, W.; Reuter, K. Water Adsorption and Dissociation on SrTiO₃(001) Revisited: A Density Functional Theory Study. *Phys. Rev. B* **2010**, *81*, 155455.

- (17) Bonnell, D. A.; Garra, J. Scanning Probe Microscopy of Oxide Surfaces: Atomic Structure and Properties. *Rep. Prog. Phys.* **2008**, *71*, 044501.
- (18) Russell, B. C.; Castell, M. R. Reconstructions on the Polar SrTiO₃(110) Surface: Analysis Using STM, LEED, and AES. *Phys. Rev. B* **2008**, *77*, 245414.
- (19) Enterkin, J. A.; Subramanian, A. K.; Russell, B. C.; Castell, M. R.; Poepelmeier, K. R.; Marks, L. D. A Homologous Series of Structures on the Surface of SrTiO₃(110). *Nat. Mater.* **2010**, *9*, 245–248.
- (20) Wang, Z.; Yang, F.; Zhang, Z.; Tang, Y.; Feng, J.; Wu, K.; Guo, Q.; Guo, J. Evolution of the Surface Structures on SrTiO₃(110) Tuned by Ti or Sr Concentration. *Phys. Rev. B* **2011**, *83*, 155453.
- (21) Li, F.; Wang, Z.; Meng, S.; Sun, Y.; Yang, J.; Guo, Q.; Guo, J. Reversible Transition Between Thermodynamically Stable Phases with Low Density of Oxygen Vacancies on the SrTiO₃(110) Surface. *Phys. Rev. Lett.* **2011**, *107*, 036103.
- (22) Biswas, A.; Rossen, P. B.; Yang, C.-H.; Siemons, W.; Jung, M.-H.; Yang, I. K.; Ramesh, R.; Jeong, Y. H. Universal Ti-rich Termination of Stomically Flat SrTiO₃(001), (110), and (111) Surfaces. *Appl. Phys. Lett.* **2011**, *98*, 051904.
- (23) Bottin, F.; Finocchi, F.; Noguera, C. Facetting and (*n*×1) Reconstructions of SrTiO₃(110) Surfaces. *Surf. Sci.* **2005**, *574*, 65 – 76.
- (24) Noguera, C.; Goniakowski, J. Polarity in Oxide Ultrathin Films. *J. Phys.: Condens. Matter.* **2008**, *20*, 264003.
- (25) Shin, J.; Nascimento, V. B.; Geneste, G.; Rundgren, J.; Plummer, E. W.; Dkhil, B.; Kalinin, S. V.; Baddorf, A. P. Atomistic Screening Mechanism of Ferroelectric Surfaces: An In Situ Study of the Polar Phase in Ultrathin BaTiO₃ Films Exposed to H₂O. *Nano Lett.* **2009**, *9*, 3720–3725.

- (26) Wang, Z.; Feng, J.; Yang, Y.; Yao, Y.; Gu, L.; Yang, F.; Guo, Q.; Guo, J. Cation Stoichiometry Optimization of SrTiO₃(110) Thin Films with Atomic Precision in Homogeneous Molecular Beam Epitaxy. *Appl. Phys. Lett.* **2012**, *100*, 051602.
- (27) Wang, Z.; Li, F.; Meng, S.; Zhang, J.; Plummer, E. W.; Diebold, U.; Guo, J. Strain-Induced Defect Superstructure on the SrTiO₃(110) Surface. *Phys. Rev. Lett.* **2013**, *111*, 056101.
- (28) Lazzeri, M.; Selloni, A. Stress-Driven Reconstruction of an Oxide Surface: The Anatase TiO₂(001)-(1×4) Surface. *Phys. Rev. Lett.* **2001**, *87*, 266105.
- (29) Blanco-Rey, M.; Abad, J.; Rogero, C.; Mendez, J.; Lopez, M. F.; Martin-Gago, J. A.; de Andres, P. L. Structure of Rutile TiO₂(110)-(1×2): Formation of Ti₂O₃ Quasi-1D Metallic Chains. *Phys. Rev. Lett.* **2006**, *96*, 055502.
- (30) Marks, L. D.; Chiamonti, A. N.; Tran, F.; Blaha, P. The Small Unit Cell Reconstructions of SrTiO₃(111). *Surf. Sci.* **2009**, *603*, 2179 – 2187.
- (31) Warschkow, O.; Wang, Y.; Subramanian, A.; Asta, M.; Marks, L. D. Structure and Local-Equilibrium Thermodynamics of the c(2×2) Reconstruction of Rutile TiO₂(100). *Phys. Rev. Lett.* **2008**, *100*, 086102.
- (32) Gong, X.-Q.; Selloni, A.; Vittadini, A. Density Functional Theory Study of Formic Acid Adsorption on Anatase TiO₂(001): Geometries, Energetics, and Effects of Coverage, Hydration, and Reconstruction. *J. Phys. Chem. B* **2006**, *110*, 2804–2811.
- (33) Blomquist, J.; Walle, L. E.; Uvdal, P.; Borg, A.; Sandell, A. Water Dissociation on Single Crystalline Anatase TiO₂(001) Studied by Photoelectron Spectroscopy. *J. Phys. Chem. C* **2008**, *112*, 16616–16621.
- (34) Yang, H. G.; Sun, C. H.; Qiao, S. Z.; Zou, J.; Liu, G.; Smith, S. C.; Cheng, H. M.; Lu, G. Q. Anatase TiO₂ Single Crystals with a Large Percentage of Reactive Facets. *Nature* **2008**, *453*, 638–641.

- (35) Selçuk, S.; Selloni, A. Surface Structure and Reactivity of Anatase TiO₂ Crystals with Dominant {001} Facets. *J. Phys. Chem. C* **2013**, *117*, 6358–6362.
- (36) Shaikhutdinov, S.; Freund, H.-J. Ultrathin Silica Films on Metals: The Long and Winding Road to Understanding the Atomic Structure. *Adv. Mater.* **2013**, *25*, 49–67.
- (37) Parkinson, G. S.; Novotný, Z.; Jacobson, P.; Schmid, M.; Diebold, U. Room Temperature Water Splitting at the Surface of Magnetite. *J. Am. Chem. Soc.* **2011**, *133*, 12650–12655.
- (38) Scheiber, P.; Riss, A.; Schmid, M.; Varga, P.; Diebold, U. Observation and Destruction of an Elusive Adsorbate with STM: O₂/TiO₂(110). *Phys. Rev. Lett.* **2010**, *105*, 216101.
- (39) Nyholm, R.; Andersen, J.; Johansson, U.; Jensen, B.; Lindau, I. Beamline I311 at MAX-LAB: a VUV/Soft X-ray Undulator Beamline for High Resolution Electron Spectroscopy. *Nucl. Instr. Meth. Phys. Res. A* **2001**, *467*, 520 – 524.
- (40) Wang, Z.; Wu, K.; Guo, Q.; Guo, J. Tuning the Termination of the SrTiO₃(110) Surface by Ar⁺ Sputtering. *Appl. Phys. Lett.* **2009**, *95*, 021912.
- (41) Sutoh, A.; Okada, Y.; Ohta, S.; Kawabe, M. Cracking Efficiency of Hydrogen with Tungsten Filament in Molecular Beam Epitaxy. *Jpn. J. Appl. Phys.* **1995**, *34*, L1379–L1382.
- (42) Kresse, G.; Hafner, J. *Ab initio* Molecular Dynamics for Open-Shell Transition Metals. *Phys. Rev. B* **1993**, *48*, 13115–13118.
- (43) Kresse, G.; Furthmüller, J. Efficiency of *ab-initio* Total Energy Calculations for Metals and Semiconductors Using a Plane-Wave Basis Set. *Comput. Mater. Sci.* **1996**, *6*, 15 – 50.
- (44) Perdew, J. P.; Burke, K.; Ernzerhof, M. Generalized Gradient Approximation Made Simple. *Phys. Rev. Lett.* **1996**, *77*, 3865–3868.
- (45) Grimme, S. Accurate Description of van der Waals Complexes by Density Functional Theory Including Empirical Corrections. *J. Comput. Chem.* **2004**, *25*, 1463–1473.

- (46) Grimme, S. Semiempirical GGA-type Density Functional Constructed with a Long-Range Dispersion Correction. *J. Comput. Chem.* **2006**, *27*, 1787–1799.
- (47) Grimme, S.; Antony, J.; Schwabe, T.; Muck-Lichtenfeld, C. Density Functional Theory with Dispersion Corrections for Supramolecular Structures, Aggregates, and Complexes of (Bio)Organic Molecules. *Org. Biomol. Chem.* **2007**, *5*, 741–758.
- (48) Klimeš, J.; Bowler, D. R.; Michaelides, A. Van der Waals Density Functionals Spplied to Solids. *Phys. Rev. B* **2011**, *83*, 195131.
- (49) Henkelman, G.; Uberuaga, B. P.; Jónsson, H. A Climbing Image Nudged Elastic Band Method for Finding Saddle Points and Minimum Energy Paths. *J. Chem. Phys.* **2000**, *113*, 9901–9904.
- (50) Sorescu, D. C.; Lee, J.; Al-Saidi, W. A.; Jordan, K. D. CO₂ Adsorption on TiO₂(110) Rutile: Insight From Dispersion-Corrected Density Functional Theory Calculations and Scanning Tunneling Microscopy Experiments. *J. Chem. Phys.* **2011**, *134*, 104707.
- (51) Thiel, P. A.; Madey, T. E. The Interaction of Water with Solid Surfaces: Fundamental Aspects. *Surf. Sci. Rep.* **1987**, *7*, 211 – 385.
- (52) Henderson, M. A. The Interaction of Water with Solid Surfaces: Fundamental Aspects Revisited. *Surf. Sci. Rep.* **2002**, *46*, 1 – 308.
- (53) Weiss, W.; Ranke, W. Surface Chemistry and Catalysis on Well-Defined Epitaxial Iron-Oxide Layers. *Prog. Surf. Sci.* **2002**, *70*, 1 – 151.
- (54) Diebold, U. The Surface Science of Titanium Dioxide. *Surf. Sci. Rep.* **2003**, *48*, 53 – 229.
- (55) Cardona, M. Optical Properties and Band Structure of SrTiO₃ and BaTiO₃. *Phys. Rev.* **1965**, *140*, A651–A655.
- (56) Cao, Y.; Wang, S.; Liu, S.; Guo, Q.; Guo, J. Electronic Structures of the SrTiO₃(110) Surface in Different Reconstructions. *J. Chem. Phys.* **2012**, *137*, 044701.

- (57) Aiura, Y.; Hase, I.; Bando, H.; Yasue, T.; Saitoh, T.; Dessau, D. Photoemission Study of the Metallic State of Lightly Electron-Doped SrTiO₃. *Surf. Sci.* **2002**, *515*, 61 – 74.
- (58) Di Valentin, C.; Tilocca, A.; Selloni, A.; Beck, T. J.; Klust, A.; Batzill, M.; Losovyj, Y.; Diebold, U. Adsorption of Water on Reconstructed Rutile TiO₂(011)-(2×1): Ti=O Double Bonds and Surface Reactivity. *J. Am. Chem. Soc.* **2005**, *127*, 9895–9903.
- (59) Henrich, V. E.; Dresselhaus, G.; Zeiger, H. J. Surface defects and the electronic structure of SrTiO₃ surfaces. *Phys. Rev. B* **1978**, *17*, 4908–4921.
- (60) D'Angelo, M.; Yukawa, R.; Ozawa, K.; Yamamoto, S.; Hirahara, T.; Hasegawa, S.; Silly, M. G.; Sirotti, F.; Matsuda, I. Hydrogen-Induced Surface Metallization of SrTiO₃(001). *Phys. Rev. Lett.* **2012**, *108*, 116802.
- (61) Meevasana, W.; King, P. D. C.; He, R. H.; Mo, S.-K.; Hashimoto, M.; Tamai, A.; Songsiriritthigul, P.; Baumberger, F.; Shen, Z.-X. Creation and Control of a Two-Dimensional Electron Liquid at the Bare SrTiO₃ surface. *Nat. Mater.* **2011**, *10*, 114–118.
- (62) King, P. D. C. et al. Subband Structure of a Two-Dimensional Electron Gas Formed at the Polar Surface of the Strong Spin-Orbit Perovskite KTaO₃. *Phys. Rev. Lett.* **2012**, *108*, 117602.
- (63) Wang, L.-Q.; Baer, D.; Engelhard, M.; Shultz, A. The Adsorption of Liquid and Vapor Water on TiO₂(110) Surfaces: the Role of Defects. *Surf. Sci.* **1995**, *344*, 237 – 250.
- (64) Ketteler, G.; Yamamoto, S.; Bluhm, H.; Andersson, K.; Starr, D. E.; Ogletree, D. F.; Ogasawara, H.; Nilsson, A.; Salmeron, M. The Nature of Water Nucleation Sites on TiO₂(110) Surfaces Revealed by Ambient Pressure X-ray Photoelectron Spectroscopy. *J. Phys. Chem. C* **2007**, *111*, 8278–8282.
- (65) Walle, L. E.; Borg, A.; Uvdal, P.; Sandell, A. Experimental Evidence for Mixed Dissociative and Molecular Adsorption of Water on a Rutile TiO₂(110) Surface Without Oxygen Vacancies. *Phys. Rev. B* **2009**, *80*, 235436.

- (66) Anisimov, V. I.; Zaanen, J.; Andersen, O. K. Band Theory and Mott Insulators: Hubbard U Instead of Stoner I . *Phys. Rev. B* **1991**, *44*, 943–954.
- (67) Cuong, D. D.; Lee, B.; Choi, K. M.; Ahn, H.-S.; Han, S.; Lee, J. Oxygen Vacancy Clustering and Electron Localization in Oxygen-Deficient SrTiO₃: LDA + U Study. *Phys. Rev. Lett.* **2007**, *98*, 115503.
- (68) Kurtz, R. L.; Stock-Bauer, R.; Msdey, T. E.; Román, E.; Segovia, J. D. Synchrotron Radiation Studies of H₂O Adsorption on TiO₂(110). *Surf. Sci.* **1989**, *218*, 178 – 200.
- (69) Di Valentin, C.; Pacchioni, G.; Selloni, A. Electronic Structure of Defect States in Hydroxylated and Reduced Rutile TiO₂(110) Surfaces. *Phys. Rev. Lett.* **2006**, *97*, 166803.
- (70) Kowalski, P. M.; Camellone, M. F.; Nair, N. N.; Meyer, B.; Marx, D. Charge Localization Dynamics Induced by Oxygen Vacancies on the TiO₂(110) Surface. *Phys. Rev. Lett.* **2010**, *105*, 146405.
- (71) Reuter, K.; Scheffler, M. Composition, Structure, and Stability of RuO₂(110) as a Function of Oxygen Pressure. *Phys. Rev. B* **2001**, *65*, 035406.
- (72) Stull, D. R.; Prophet, H. *JANAF Thermochemical Tables*, 2nd ed.; U.S. Dept. of Commerce, National Bureau of Standards Washington, D.C, 1971.
- (73) Merte, L. R.; Peng, G.; Bechstein, R.; Rieboldt, F.; Farberow, C. A.; Grabow, L. C.; Kudernatsch, W.; Wendt, S.; Lægsgaard, E.; Mavrikakis, M.; Besenbacher, F. Water-Mediated Proton Hopping on an Iron Oxide Surface. *Science* **2012**, *336*, 889–893.
- (74) Wendt, S.; Matthiesen, J.; Schaub, R.; Vestergaard, E. K.; Lægsgaard, E.; Besenbacher, F.; Hammer, B. Formation and Splitting of Paired Hydroxyl Groups on Reduced TiO₂(110). *Phys. Rev. Lett.* **2006**, *96*, 066107.
- (75) Lu, G.; Linsebigler, A.; Yates, J. T. Ti³⁺ Defect Sites on TiO₂(110): Production and Chemical Detection of Active Sites. *J. Phys. Chem.* **1994**, *98*, 11733–11738.

- (76) Chambers, S.; Ohsawa, T.; Wang, C.; Lyubinetsky, I.; Jaffe, J. Band Offsets at the Epitaxial Anatase $\text{TiO}_2/n\text{-SrTiO}_3(001)$ Interface. *Surf. Sci.* **2009**, *603*, 771 – 780.
- (77) Abad, J.; Böhme, O.; Román, E. Dissociative Adsorption of NO on $\text{TiO}_2(110)\text{-}(1\times 2)$ Surface: Ti_2O_3 Rows as Active Sites for the Adsorption. *Langmuir* **2007**, *23*, 7583–7586.

Table 1: Oxygen vacancy formation energy $E_f(V_O)$ and hydrogen adsorption energy $E_{ads}(H)$ (in eV) for different oxygen sites (following the labeling given in Fig. 1b) obtained with the PBE functional. Numbers in brackets refer to the relative energy with respect to the most stable configuration. For geometries of adsorbed H see the Supplement.

	O1	O2	O3	O4	O5
V_O formation energy (eV)	6.43 (0.83)	5.95 (0.35)	5.60 (0.0)	5.68 (0.08)	5.76 (0.16)
H adsorption energy (eV)	1.79 (-0.40)	1.93 (-0.26)	2.19 (0.0)	2.16 (-0.03)	1.62 (-0.57)

Table 2: Calculated water adsorption energies $E_{ads}(H_2O)$ (in eV), bond lengths (\AA) (O_W and O_S denotes O atoms in the water molecule and surface, respectively), and $H-O_W-H$ angles ($^\circ$) for molecular adsorption configurations on the defective surface, calculated with different functionals.

Functional	$E_{ads}(H_2O)$	Ti- O_W	H- O_W	H- O_S	H- O_W -H
PBE	-1.732	2.107, 3.090	1.055, 0.985	1.571	109.22
DFT-D2	-1.857	2.102, 3.061	1.057, 0.985	1.560	109.31
vdW-DFT	-1.727	2.098, 3.167	1.059, 0.987	1.552	109.35

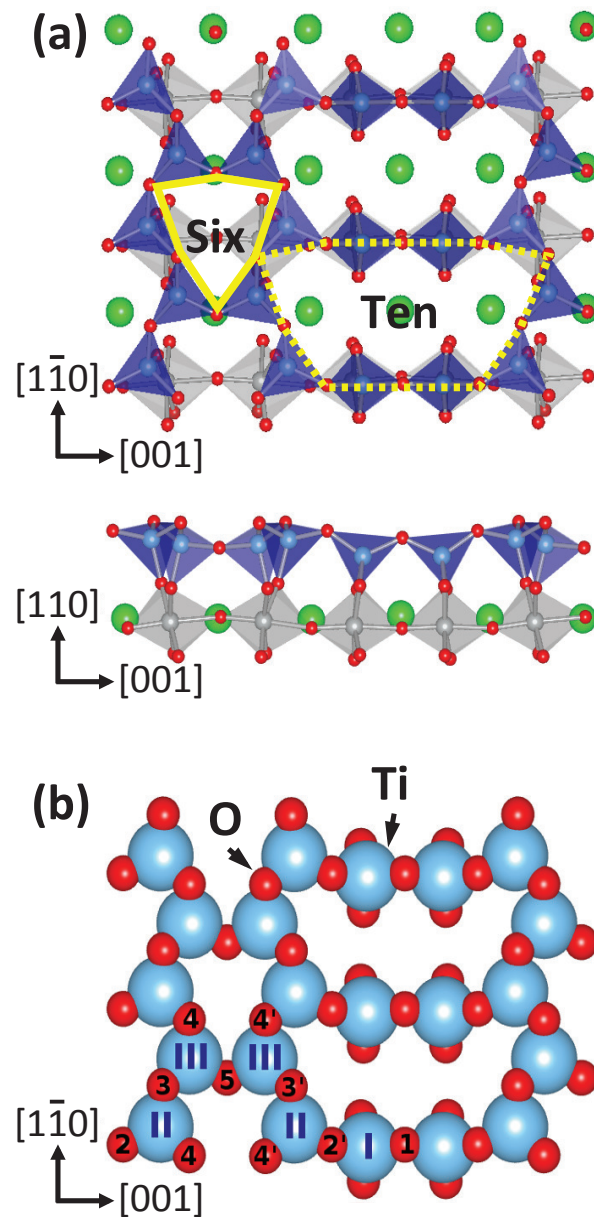


Figure 1: Model of the SrTiO₃(110)-(4 × 1) surface. (a) Top and side views. The reconstructed layer consists of a network of darker TiO₄ tetrahedra (blue) forming six- and ten-membered rings, on top of the SrTiO₃(110) substrate, which contains TiO₆ octahedra (lighter, gray). Large, medium and small spheres denote Sr, Ti and O atoms, respectively. (b) Top view of the topmost reconstructed layer with the surface Ti and O atoms labels used in the present study.

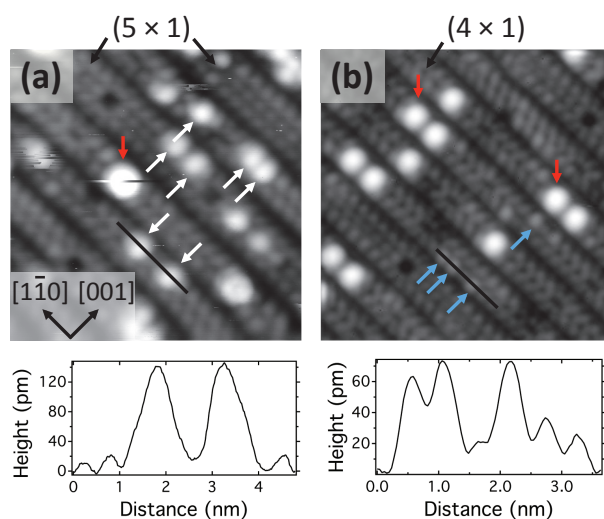


Figure 2: STM images (image size $9 \times 9 \text{ nm}^2$, sample bias $+2.3 \text{ V}$, tunneling current 0.1 nA) of the $\text{SrTiO}_3(110)$ surface. The surface exhibits an overall (4×1) reconstruction; locally a few (5×1) rows are apparent. (a) After exposure to atomic hydrogen and (b) after flashing the surface in (a) to $\sim 300 \text{ }^\circ\text{C}$. Sr adatoms, hydroxyls and oxygen vacancies appear in various levels of brightness and are labeled by red, white and blue arrows, respectively. The line profiles in the lower panels were taken at the lines shown in the STM images.

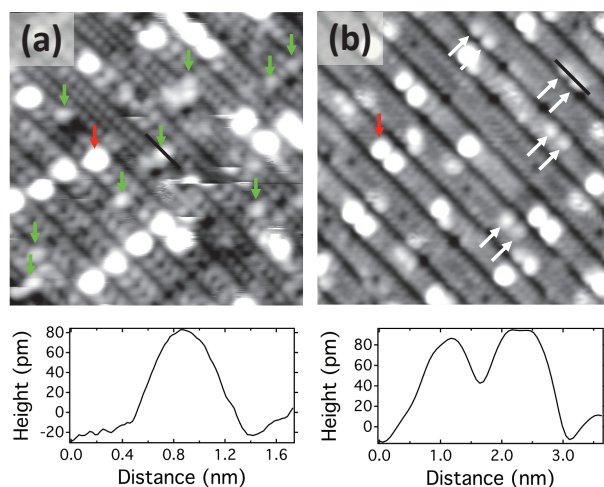


Figure 3: STM images ($18 \times 18 \text{ nm}^2$, 2.1 V , 0.1 nA) of the $\text{SrTiO}_3(110)-(4 \times 1)$ surface after exposure to (a) 0.3 L water at 110 K , imaged at 78 K ; (b) 3 L at RT , imaged at RT . Green and white arrows point to molecular water and hydroxyl pairs, respectively. As in Fig. 2 the red arrows point out single Sr adatoms. The line profiles in the lower panels were taken at the lines shown in the STM images.

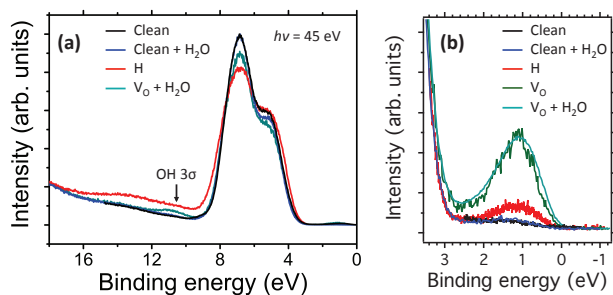


Figure 4: Comparison of valence band photoemission spectra of the clean surface (black), after exposure to water (blue), atomic hydrogen (red), of a surface with oxygen vacancies (green), and after exposure to water (cyan). All spectra were taken at RT.

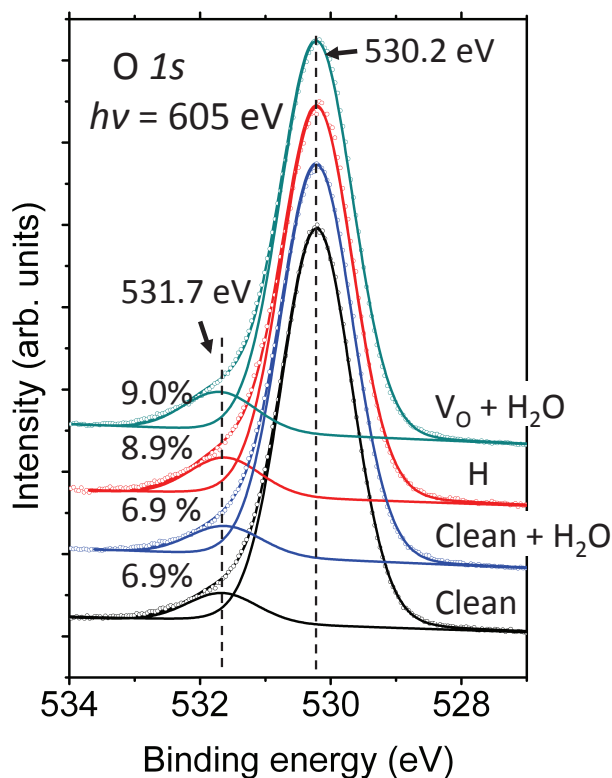


Figure 5: Comparison of O 1s core-level XPS spectra of the clean surface (black), after exposure to water (blue) and atomic hydrogen (red), and surface with oxygen vacancies exposed to water (cyan). All spectra were taken at RT.

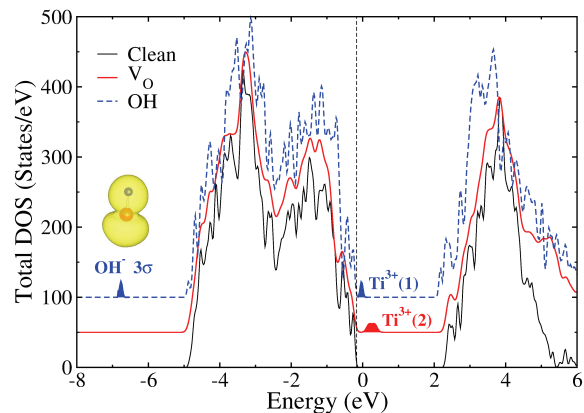


Figure 6: PBE+ U valence and conduction band density of states of the clean SrTiO₃(110)-(4 × 1) surface (thin black line) and the reduced surface with an oxygen vacancy (red full line) and hydroxyl species (dashed blue line). All spectra are aligned with respect to their valence-band maxima. The Ti³⁺ midgap states [both singly, Ti³⁺ (1), and doubly, Ti³⁺ (2) occupied] as well as the OH-3 σ states are highlighted with a colored background.

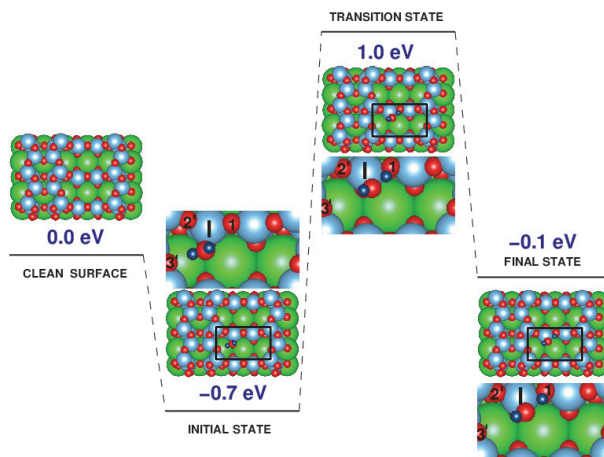


Figure 7: Potential-energy profile for the reaction of an adsorbed H₂O molecule on the ideal, non-defective SrTiO₃(110)-(4 × 1) surface. The energy zero corresponds to the H₂O in the gas phase far away from the surface. For each state considered the corresponding optimized structures are shown as insets in wide and zoomed view.

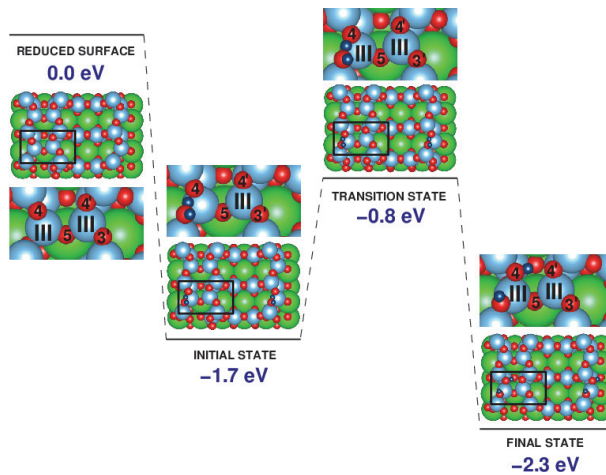


Figure 8: Potential-energy profile for the reaction of an adsorbed H₂O molecule at the defective SrTiO₃(110)-(4 × 1) surface. The energy zero corresponds to the H₂O in the gas phase, far away from the surface.